Dynamics of Bullet Shaped Bubbles Encountered in Vertical Gas Liquid Slug Flow

JAMES R. STREET and M. RASIN TEK

The University of Michigan, Ann Arbor, Michigan

A theoretical analysis is presented of the liquid film flowing around long, bullet shaped, gas bubbles which characterize the slug-flow regime in two-phase flow through vertical pipe. Integral mass and momentum balances on the liquid film allow the prediction of gas bubble shape, liquid holdup around the bubble, wall shear stress acting on the liquid film, and velocity profiles in the liquid film. These predictions are in good agreement with data available in the literature.

If a sufficient quantity of gas is introduced into a stagnant liquid column or a flowing liquid stream, a bullet shaped bubble is formed. The consecutive passage of these bubbles up a circular pipe characterizes the slug-flow regime of vertical two-phase flow. Previous studies of these bubbles by various investigators (*1, 2, 3, 4, 5, 6, 7*) have been concerned primarily with the prediction and correlation of bubble rise velocities. Bretherton (*8*) has investigated theoretically the shapes of bubbles moving slowly in horizontal and vertical capillaries in which the forces of surface tension and viscosity were included for the horizontal case and surface tension and gravity for the vertical case. Walters and Davidson (*9, 10*) have investigated the initial motion of cylindrical (two-dimensional) and spherical (three-dimensional) bubbles when released from rest in a vertical conduit. In the latter case they predicted and observed the deformation of the bubble from a sphere to a spherical cap. Taylor and Acrivos (*11*) have investigated theoretically the slow, creeping motion of a fluid around a viscous, deformable drop. Their analysis revealed that the drop would deform from a sphere to a spherical cap as the fluid velocity (and therefore inertial terms) increased in magnitude. Brown (*12*) extended earlier work (*1, 2*) to include the effects of liquid viscosity on the velocity of bullet shaped bubbles.

The objective of this study is to examine the fluid mechanics of the liquid film which flows downward with respect to the bubble, around the bubble, forming a wake behind it as indicated in Figure 1. Integral mass and momentum balances on this film allow estimations of the bubble shape, liquid holdup around the bubble, wall shear acting on the liquid film, and velocity profiles in the liquid film. The predictions of the theory are in good agreement with the experimental data of Nicklin (*5*) and Laird and Chisholm (*4*). The unique features of this analysis are that the flow around the bubble is analyzed at the bubble terminal velocity, where the nonlinear inertial forces may be quite large. Secondly, the analysis is not restricted to bubbles rising through a stagnant liquid. Finally, the momentum balance is formulated in such a manner as to continuously analyze the forces in the liquid film along the length of the bubble as opposed to those analyses which comprised an inertia-gravity controlled solution at the head of the bubble, which may or may not be patched to a viscosity-gravity controlled solution in the film at the tail of the bubble.

James R. Street is with Shell Development Company, Emeryville, California.

THEORETICAL ANALYSIS

It will be assumed in this analysis that predictive methods or correlations are available for the estimation of bubble rise velocity. The bubble rise velocity is expressed in the form

$$v_B = v_G + v_L + w \qquad (1)$$

The regions of the pipe occupied by the liquid phase are assumed to travel at a superficial velocity equal to $v_G + v_L$; therefore, w is interpreted as the velocity with which the gas bubble travels through the surrounding liquid. It is this quantity which is of paramount interest.

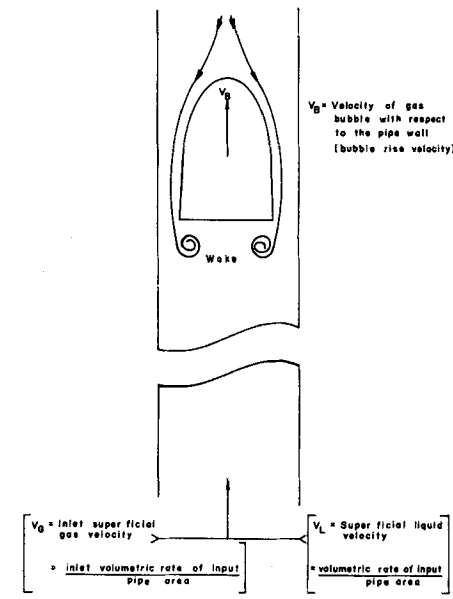

Fig. 1. Schematic representation of a rising gas bubble.

Integral Mass and Momentum Balances

Let a differential element of liquid film located a distance z from the head of the bubble be taken as the system under consideration (the element *CDEFGHIJ* in Figure 2). This system is allowed to move with the bubble at the bubble rise velocity which is assumed constant. A mass balance yields

$$\frac{\partial}{\partial z}\int_{r_G}^{r_W} u r dr = 0 \tag{2}$$

where u, the velocity in the z direction, is a function of r and z. A mass balance on the system *ABEFIJ* yields

$$\int_{r_G}^{r_W} u r dr = w r_W^2/2 \tag{3}$$

A momentum balance on the differential element dz yields

$$-\frac{\partial}{\partial z}\int_{r_G}^{r_W} \rho u^2 2\pi r dr + \mu 2\pi r_W \frac{\partial u}{\partial r}\bigg|_{r=r_W} + \rho\pi g(r_W^2 - r_G^2) - \pi k\sigma r_W \frac{d\beta}{dz} = 0 \tag{4}$$

The terms in Equation (4) take into account liquid acceleration and the forces due to viscous wall shear, gravity, and surface tension, respectively.

It is assumed that the pressure gradient across the gas bubble is negligibly small. This has been observed experimentally by Laird and Chisholm (*4*) for a gas bubble rising through a stagnant liquid. Furthermore, it is assumed that at the gas-liquid interface

$$\frac{\partial u}{\partial r}(r_G, z) = 0 \tag{5}$$

Thus the transfer of momentum from the gas bubble to the liquid film is assumed to have a negligible effect on the fluid mechanics of the film. This assumption appears not to invalidate the model for the bullet shaped bubbles which travel through the liquid at moderate velocities. As the gas bubbles travel through the liquid at higher and higher velocities (for example, annular gas flow), this assumption can be expected to be limiting.

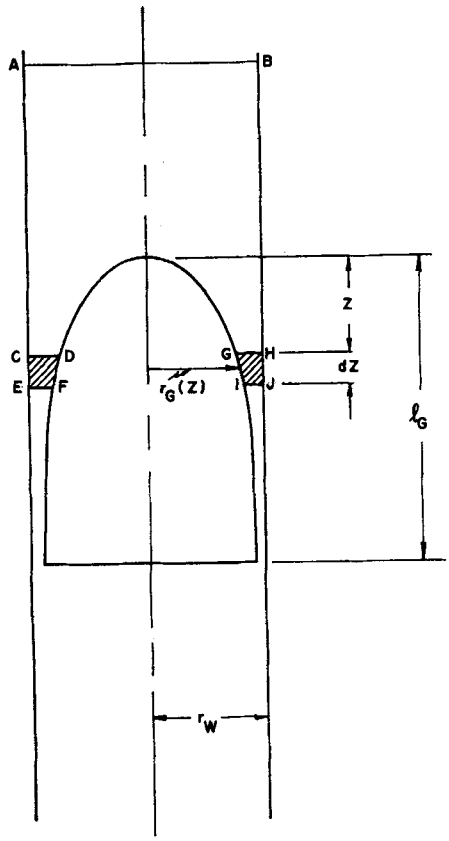

Fig. 2. Mathematical model of a rising gas bubble.

A final condition may be imposed on the liquid film, namely, the condition of nonslip at the pipe wall:

$$u(r_W, z) = v_G + v_L + w \tag{6}$$

Equations (3) through (6) may be put in dimensionless form and expressed in terms of the minimum number of parameters by the method of Hellums and Churchill (*13*). The resulting equations are

$$\int_{\sqrt{\beta}}^{1} u_D \eta d\eta = 1/2\,\frac{w}{v_G + v_L + w} \tag{7}$$

$$\frac{\partial}{\partial z_D}\int_{\sqrt{\beta}}^{1} u_D^2 \eta d\eta - \frac{N_{Fr}}{N_{Re}}\frac{\partial u_D}{\partial \eta}\bigg|_{\eta=1} - \left(\frac{1-\beta}{2}\right) + \left(\frac{k}{2N_{We}}\right)\frac{d\beta}{dz_D} = 0 \tag{8}$$

where

$$u_D = u/v_G + v_L + w, \quad z_D = zg/(v_G + v_L + w)^2, \quad \eta = r/r_W$$

$$r_G = \sqrt{\beta}\, r_W,$$

N_{Fr} = Froude number $= (v_G + v_L + w)^2/gr_W$

N_{Re} = Reynolds number $= r_W(v_G + v_L + w)\rho/\mu$,

N_{We} = Weber number $= (v_G + v_L + w)^2\rho r_W/\sigma$

Second

$$\frac{\partial u_D}{\partial \eta}(\sqrt{\beta}, z_D) = 0 \tag{9}$$

$$u_D(1, z_D) = 1 \tag{10}$$

The integral form of the mass and momentum equations requires that a functional form of the velocity profile be assumed in order that Equations (7) through (10) be solved. Therefore, let a general velocity profile subject to the three conditions (7), (9), and (10) be assumed in the form

$$u_D(\eta, z_D) = f_1(\beta)F_1(\eta) + f_2(\beta)F_2(\eta) + f_3(\beta)F_3(\eta) \tag{11}$$

If the functions $F_1(\eta)$, $F_2(\eta)$, and $F_3(\eta)$ are arbitrarily specified, then $f_1(\beta)$, $f_2(\beta)$, and $f_3(\beta)$ are determined by (7), (9), and (10). Substitution of (11) in (8) then yields

$$F(\beta, V)\frac{d\beta}{dz_D} - \frac{N_{Fr}}{N_{Re}}H(\beta) - \left(\frac{1-\beta}{2}\right) + \left(\frac{k}{2N_{We}}\right)\frac{d\beta}{dz_D} = 0 \tag{12}$$

where

$$V = w/v_G + v_L + w \tag{13}$$

$$\frac{\partial}{\partial z_D}\int_{\sqrt{\beta}}^{1} u_D^2 \eta d\eta = F(\beta, V)\frac{d\beta}{dz_D} \tag{14}$$

and

$$\frac{\partial u_D}{\partial \eta}\bigg|_{\eta=1} = H(\beta) \tag{15}$$

The differential Equation (12) may be solved to yield

$$z_D = \int_0^{\beta} \frac{F(\beta, V) + \dfrac{k}{2N_{We}}}{\left[\ (1-\beta)/2 + \dfrac{N_{Fr}}{N_{Re}} H(\beta)\ \right]} d\beta \quad (16)$$

where $\beta(z_D) = 0$ at $z_D = 0$. Equation (16) may be expressed more compactly in the form

$$z_D = \int_0^{\beta} G\left(\beta, V, \frac{N_{We}}{k}, \frac{N_{Fr}}{N_{Re}}\right) d\beta \quad (17)$$

The function G will be referred to as $G(\beta)$ in the sequel.

Equation (17) allows the prediction of gas bubble shape and (11) the estimation of velocity profiles in the liquid film. The cumulative volumetric liquid holdup around the gas bubble is given as a function of bubble length by

$\lambda \equiv$ cumulative volumetric holdup of liquid/cross-sectional pipe area

$$= \int_0^{z} [1 - \beta(z)]dz = \int_0^{\beta} (1-\beta)\, G(\beta)\, d\beta \quad (18)$$

The cumulative viscous shear acting on the liquid film at the wall is defined as the total shear force acting on the film at the wall divided by the cross-sectional pipe area

$$F_W = -\frac{2\mu(v_G + v_L + w)}{\rho r_w^2 g} \int_0^{z} \left(\frac{\partial u_D}{\partial \eta}\right)_{\eta=1} dz \quad (19)$$

which may be written as

$$F_W = -\frac{2\mu(v_G + v_L + w)}{r_w^2 \rho g} \int_0^{\beta} H(\beta)\, G(\beta)\, d\beta \quad (20)$$

Liquid Film Velocity Profiles

The effects on bubble shape were investigated for three functional forms of $u_D(\eta, z_D)$; namely

$$u_D = \phi(\eta)$$

$$u_D = \phi(z_D)$$

and

$$u_D = \phi(\eta, z_D) = f_1(\beta)\eta^2 + f_2(\beta)\eta^4 + f_3(\beta)\eta^6$$

For the case in which the velocity in the film is a function of η only, the mass balance (7) can be evaluated from Liebnitz' rule. The result is

$$\frac{d\beta}{dz_D} = 0, \quad \beta = \text{constant}$$

The bubble is therefore cylindrical in shape. The dimensionless area of the bubble is given by substitution for u_D in (8):

$$\frac{N_{Fr}}{N_{Re}} \frac{\partial u_D}{\partial \eta}\bigg|_{\eta=1} + \frac{1-\beta}{2} = 0 \quad (21a)$$

or

$$\beta = 1 + \frac{2N_{Fr}}{N_{Re}} \phi'(1) \quad (21b)$$

Because $\beta \leq 1$, $\phi'(1) \leq 0$, which implies that the fluid in the film must be traveling downward with respect to the pipe wall. If u_D is neither a function of η nor z_D, $\phi'(1) = 0$ and $\beta = 1$; that is, the gas bubble is a cylinder occupying the entire cross section of the pipe.

For the case in which the velocity in the film is a function of z_D only, the mass balance (7) becomes

$$(1-\beta)\frac{du_D}{dz_D} - u_r \frac{d\beta}{dz_D} = 0 \quad (22)$$

The momentum balance (8) becomes

$$\frac{d}{dz_D}\left[u_D^2\left(\frac{1-\beta}{2}\right)\right] - \left(\frac{1-\beta}{2}\right) + \frac{k}{2N_{We}}\frac{d\beta}{dz_D} = 0 \quad (23)$$

Equations (22) and (23) can be combined by elimination of u_D to give

$$(1-\beta)^2 \frac{d^2\beta/dz_D^2}{(d\beta/dz_D)^2} + 3(1-\beta) - \frac{2k}{N_{We}}\frac{d\beta}{dz_D} = 0 \quad (24)$$

This equation is solved by

$$\beta(z_D) = 1 - e^{-\frac{N_{We}}{k} z_D} \quad (25)$$

which satisfies the initial condition $\beta(0) = 0$. For this case then the bubble shape is exponential. The bubble surface asymptotically approaches the wall as z_D approaches infinity.

Finally the velocity in the film is taken as a function of both η and z_D. The first three terms of an even power series in η were taken because at the bubble head $\beta = 0$ the film velocity is an even function of η. The conditions (7), (9), and (10), when combined with the specific form of (11) used, yield the following expressions for $f_1(\beta)$, $f_2(\beta)$, and $f_3(\beta)$:

$$f_1 = \frac{\beta}{1-2\beta}[-2 + (2-3\beta)f_3] \quad (26a)$$

$$f_2 = \frac{1 + (3\beta^2 - 1)f_3}{1-2\beta} \quad (26b)$$

$$f_3 = \frac{12[V(1-2\beta) + (\beta - 1/3 - 2/3\,\beta^3)]}{-1 + 6\beta - 6\beta^2 - 8\beta^3 + 15\beta^4 - 6\beta^5} \quad (26c)$$

Equations (26) specify $u_D(\eta, z_D)$ which give upon substitution in (14)

$$F(\beta) = f_1 f_1'\left(\frac{1-\beta^3}{3}\right) + (f_1 f_2' + f_2 f_1')\left(\frac{1-\beta^4}{4}\right)$$
$$+ (f_2 f_2' + f_1 f_3' + f_1' f_3)\left(\frac{1-\beta^5}{5}\right) + (f_2' f_3 + f_2 f_3')\left(\frac{1-\beta^6}{6}\right)$$
$$+ f_3 f_3'\left(\frac{1-\beta^7}{7}\right) - 1/2\,[f_1^2\beta^2 + 2f_1 f_2\beta^3 + (f_2^2 + 2f_1 f_3)\beta^4$$
$$+ 2f_2 f_3\beta^5 + f_3^2\beta^6] \quad (27)$$

where

$$f_1' = \frac{df_1}{d\beta} = \frac{1}{1-2\beta}\left(\frac{f_1}{\beta} + \beta\,[(2-3\beta)\,f_3' - 2f_3]\right) \quad (28a)$$

$$f_2' = \frac{df_2}{d\beta} = \frac{1}{1-2\beta}\,[(3\beta^2 - 1)\,f_3' + 6\beta f_3 + 2f_2] \quad (28b)$$

$$f_3' = \frac{df_3}{d\beta} = \frac{12}{X}\left[\ (2V - 1 + 2\beta^3) - \frac{6AY}{X}\ \right] \quad (28c)$$

and

$$A = V(2\beta - 1) + 1/3 - \beta + 2/3\,\beta^3 \quad (29a)$$

$$X = 1 - 6\beta + 6\beta^2 + 8\beta^3 - 15\beta^4 + 6\beta^5 \quad (29b)$$

$$Y = 1 - 2\beta - 4\beta^2 + 10\beta^3 - 5\beta^4 \quad (29c)$$

Finally substitution for u_D in (15) yields

$$\frac{\partial u_D}{\partial \eta}\bigg|_{\eta=1} = H(\beta) = 2f_1 + 4f_2 + 6f_3 \quad (30)$$

Substitution of Equations (26) through (30) allows the calculation of the bubble shape (β as a function of z).

TABLE 1. SUMMARY OF DATA FOR NUMERICAL EXAMPLES

	Numerical example of Nicklin	Numerical example of Laird & Chisholm	Numerical example of Fig. 9
r_W, cm.	1.29	2.54	2.86
$v_G + v_L$, cm./sec.	0.0	0.0	100.0
w, cm./sec.	17.3	25.3	63.0
ρ, g./cc.	1.0	1.0	1.0
μ, centipoises	1.0	1.0	1.0
σ, dynes/cm.	72.8	72.8	72.8
k	1.0	1.0	1.0
g, cm./sec.^{2}	980.0	980.0	980.0

Because of the complicated form of the integrand in (16), an analytical solution was not obtained. Rather, the integration was performed numerically on a digital computer for specific cases to be presented.

Considerations of Dimensional Analysis

Equations (7) through (10) indicate that

$$\beta = \Phi\left(V, \frac{N_{We}}{k}, z_D, \frac{N_{Fr}}{N_{Re}}\right) \tag{31}$$

If a mean value of β is defined by

$$\beta_M = \frac{1}{l_G}\int_o^{l_G} \beta(z)\, dz \tag{32}$$

then (31) becomes

$$\beta_M = \Phi\left(V, \frac{N_{We}}{k}, \frac{N_{Fr}}{N_{Re}}, \frac{gl_G}{(v_G + v_L + w)^2}\right) \tag{33}$$

where the group $(v_G + v_L + w)^2/gl_G$ is a Froude number based on gas bubble length.

For long gas bubbles rising through a stagnant liquid for which the effects of surface tension are negligible, (33) reduces to

$$\beta_M = \Phi\left[\frac{N_{Fr}}{N_{Re}}\right] \tag{34}$$

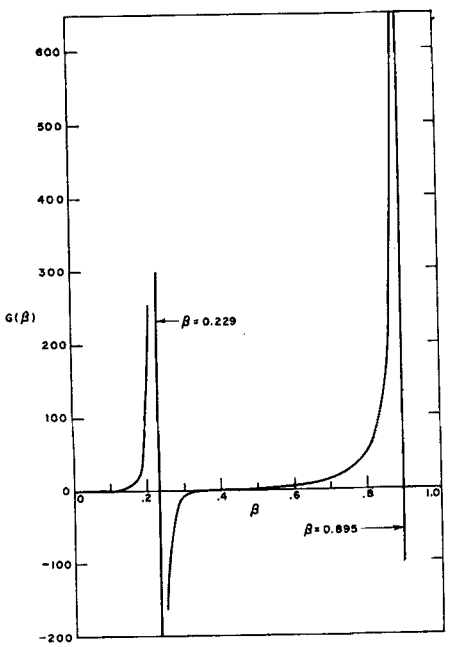

Fig. 3. The function $G(\beta)$ for the numerical example of Nicklin.

or

$$\frac{\mu w}{\rho r_W^2 g} = \Psi(\beta_M) \tag{35}$$

where $\Psi(\beta_M)$ is a function of the bubble geometry. This result corresponds to the theoretical predictions of Dumitrescu (2) and Davies and Taylor (1) who obtained for an a priori specification of bubble shape:

$$w = C\sqrt{gD} \tag{36}$$

If arbitrarily one sets $\Psi(\beta_M) = C' r_W^{-3/2}$ and $C' = \sqrt{2/g}\,(C\mu/\rho)$, then (35) reduces to (36). Thus the constant C in (36) should be a function of the physical properties of the liquid, a result which has been experimentally verified by White and Beardmore (7) and Brown (12).

If the restriction of a stagnant liquid is removed, (33) reduces to

$$V = \Psi\left(\beta_M, \frac{N_{Fr}}{N_{Re}}\right) \tag{37}$$

This expression corresponds to the results of Nicklin (5) and Griffith and Wallis (3) who obtained correlations for the bubble-rise velocity for an air-water system in the general form

$$w = C_1\sqrt{gD} + C_2\,(v_G + v_L) \tag{38}$$

The correspondence can be demonstrated by substitution in (37) for β_M by (34) and (36):

$$V = \Psi\left[C\sqrt{gD}, \frac{\mu}{\rho r_W^2 g}(v_G + v_L + w)\right] \tag{39}$$

And for a given gas-liquid system

$$w = \Psi\left[\sqrt{gD}, (v_G + v_L)\right] \tag{40}$$

Finally, the Froude number based on bubble length in (33) indicates that the bubble velocity should be a function of bubble length, a result which has been confirmed experimentally by Laird and Chisholm (4) and Nicklin (5).

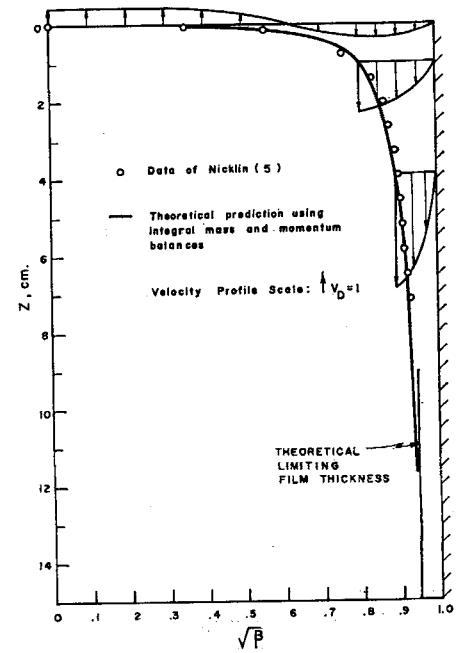

Fig. 4. Bubble shape ($\sqrt{\beta}$ vs. Z) and velocity profiles in the liquid film for the numerical example of Nicklin.

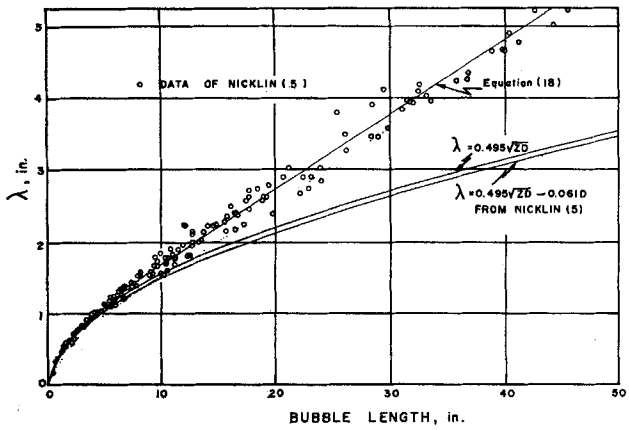

Fig. 5. Cumulative holdup in the liquid film vs. bubble length for the numerical example of Nicklin.

These considerations indicate that [in the sense of (33), (35), and (40)] the functional dependence of bubble-rise velocity as predicted by the model presented here agrees with the experimental observations of many investigators (*1, 2, 3, 4, 5, 7*). This qualitative correspondence would appear to lend credence to the theoretical analysis.

RESULTS AND COMPARISONS WITH EXPERIMENTAL DATA

Experimental data of Nicklin (5) and Laird and Chisholm (*4*), who studied air bubbles rising through a stagnant column of water in pipes of 1.29- and 2.54-cm. radius, respectively, have been compared with the theoretical predictions of this model. In addition examples are presented of predictions of bubble shape and velocity profiles for a bubble rising through a continuously flowing liquid. The specific data used for these three numerical examples are presented in Table 1. In all cases u_D was taken as a function of η and z_D in the manner prescribed by Equation (11) and Equations (26) through (30).

A typical example of $G(\beta)$ as a function of β is presented in Figure 3 for the numerical example of Nicklin. The singularity at $\beta = 0.229$ indicates the existence of a second solution for bubble shape for bubbles of small areal extent. From experimental observations it is known that bubbles of small areal extent are approximately spherical in shape. The approximate expression used here for the velocity profile, however, does not allow prediction of this spherical shape.

The singularity in $G(\beta)$ at $\beta = 0.895$ predicts that the film will attain a limiting thickness given by a balance of wall shear and gravity forces. The thickness is predicted by Equations (21). Moreover, even if the gas bubble is

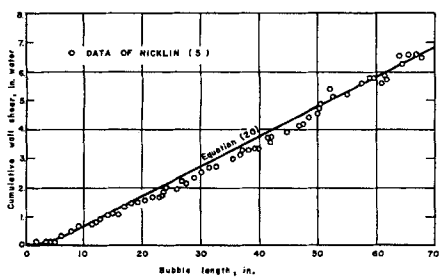

Fig. 6. Cumulative wall shear acting on the liquid film vs. bubble length for the numerical example of Nicklin.

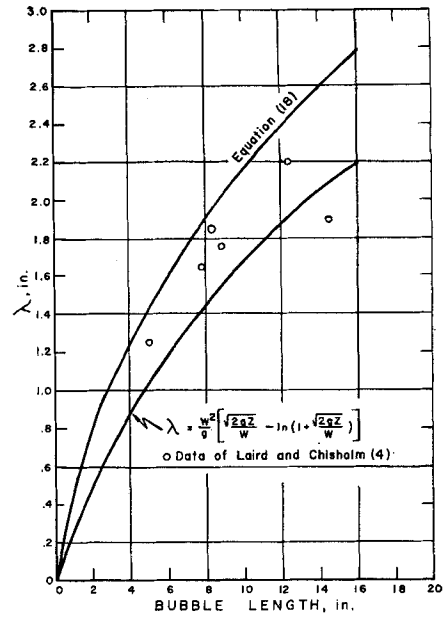

Fig. 7. Cumulative holdup in the liquid film vs. bubble length for the numerical example of Laird and Chisholm.

infinitely long, a thin film of liquid will adhere to the pipe wall. This is precisely the phase configuration called *annular flow*. Because interfacial shear is neglected here, no quantitative information can be gained into the transition process from the slug flow regime to the annular flow regime. However, the slug flow regime and the annular flow regime differ in that the velocity profiles in the thin film in slug flow are directed downward with respect to the pipe wall, whereas in annular flow the velocity profiles are directed upward. Therefore a transition flow regime must exist to effect a change in the direction of the liquid-film velocity profiles through the mechanism of interfacial shear. It is known experimentally that this flow regime is not well defined geometrically and consists of many regions of upward and downward flow such that considerable depletion and regeneration of these two types of flow occur.

Figure 4 contains a comparison between the predicted bubble shape and the bubble shape measured from a

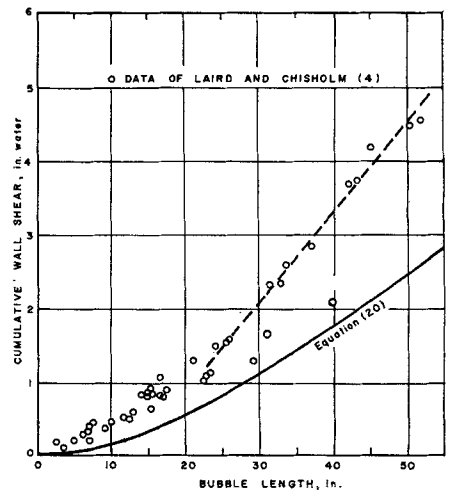

Fig. 8. Cumulative wall shear acting on the liquid film vs. bubble length for the numerical example of Laird and Chisholm.

photograph of Nicklin (5). The velocity profiles presented are those measured with respect to the pipe wall:

$$v_D = [(u - (v_G + v_L + w)]/(v_G + v_L + w) = u_D - 1 \quad (41)$$

The unidirectional nature of the wall shear agrees directly with the data of Nicklin.

Figures 5 and 6 compare the theoretical predictions of cumulative liquid holdup and cumulative wall shear with the data of Nicklin (5). The theoretical predictions of Nicklin are plotted in Figure 5.

The limiting values of the slopes of the lines in Figures 5 and 6 correspond to the conditions in the limiting film:

$$\left(\frac{d\lambda}{dz}\right)_{11m} = (1-\beta)_{11m} \quad (42)$$

$$\left(\frac{dF_w}{dz}\right)_{11m} = -\frac{2\mu(v_G + v_L + w)}{\rho r_w^2 g}(2f_1 + 4f_2 + 6f_3)_{11m} \quad (43)$$

and

$$\left(\frac{d\lambda}{dz}\right)_{11m} = \left(\frac{dF_w}{dz}\right)_{11m} = \begin{cases} 0.102 & \text{experimental from Nicklin (5)} \\ 0.105 & \text{theoretical from this work} \end{cases}$$

Figures 7 and 8 compare the theoretical predictions of cumulative liquid holdup and cumulative wall shear with the data of Laird and Chisholm (4). Their theoretical prediction of liquid holdup is presented in Figure 7, which neglects wall shear and surface tension and does not extend to continuously flowing liquid systems. Although these investigators did not recognize the existence of a limiting film thickness in their paper, a straight line drawn through their data as indicated in Figure 8 yields the following comparison:

$$\left(\frac{dF_w}{dz}\right)_{11m} = \begin{cases} 0.12 & \text{experimental from data of Laird and Chisholm (4)} \\ 0.07 & \text{theoretical from this work} \end{cases}$$

The low values predicted for cumulative wall shear and limiting film thickness are probably due to the approximate nature of the velocity profiles used.

One of the distinguishing features of the model presented here is its ability to predict bubble shape, wall shear, etc. for pipes in which a continuous flow of gas and liquid is occurring. A numerical example of the prediction of bubble shape is presented in Figure 9 for the data in Table 1. Examples of the velocity profiles are also presented. This example shows the streamlining effect of higher bubble-rise velocities on the bubble shape. In addition, the bidirectional nature of the velocity profiles and wall shear becomes apparent. The solid line drawn in Figure 9 at $z = 12.5$ cm. indicates the location at which the velocities in the liquid film are zero with respect to the pipe wall.

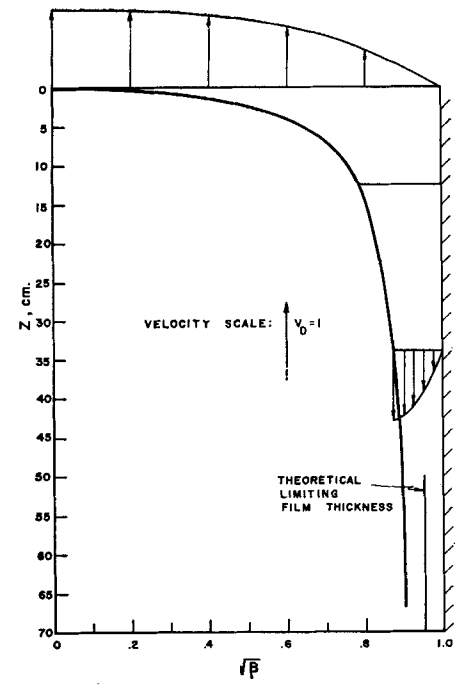

Fig. 9. Bubble shape ($\sqrt{\beta}$ vs. Z) and velocity profiles in the liquid film in a continuously flowing air-water system.

SUMMARY

1. Integral mass and momentum balances on the liquid film flowing around the bullet shaped bubbles which characterize slug flow allow the prediction of bubble shape, liquid holdup around the bubble, viscous wall shear, and velocity profiles in the liquid film.

2. This analysis extends the work of previous investigators (4, 5) to include viscous effects in the liquid film, the effects of surface tension, and effects of a continuously flowing liquid stream.

3. Dimensional analysis of the equations developed indicates a functional dependence of the bubble-rise velocity of the form observed experimentally by many investigators.

4. The theoretical predictions are in good agreement with the data for bubble shape, liquid holdup, and wall shear of Nicklin (5) and Laird and Chisholm (4) for air bubbles rising through a column of stagnant water.

In conclusion, it is perhaps appropriate to state an application of this theory to the theory of slugging gas-liquid systems as devised by Street and Tek (6). In analyzing slug flow, one need only treat the gas bubble regions as regions of constant pressure. This means that the effects of acceleration of liquid around a gas bubble cannot be neglected. In the analysis of slug flow one need not worry about liquid holdup around a bubble or wall shear; one need only recognize the fact that the combined effects of liquid acceleration, surface tension, wall shear, and liquid holdup are self-cancelling.

ACKNOWLEDGMENT

James R. Street would like to thank the National Science Foundation for financial support in the form of two NSF Fellowships.

NOTATION

D = pipe diameter
$f_{1,2,3}$ = functions defined by (11)
$F_{1,2,3}$ = functions defined by (11)
F = function defined by (14)
F_W = cumulative wall shear
g = acceleration of gravity
G = function defined by (17)
H = function defined by (15)
k = constant in surface tension force
l_G = length of gas bubble
N_{Fr} = Froude number, $(v_G + v_L + w)^2/gr_W$
N_{Re} = Reynolds number, $r_W(v_G + v_L + w)\rho/\mu$
N_{We} = Weber number, $(v_G + v_L + w)^2\rho r_W/\sigma$

P = pressure
r = radius
r_G = radius at which gas-liquid interface is located
r_W = pipe radius
u = velocity in liquid film measured with respect to gas bubble
u_D = dimensionless velocity, $u/(v_G + v_L + w)$
v = velocity in liquid film measured with respect to pipe wall
v_B = bubble-rise velocity
v_G = superficial gas velocity
v_L = superficial liquid velocity
V = dimensionless velocity, $w/(v_G + v_L + w)$
w = velocity of gas bubble through surrounding liquid
z = vertical distance from bubble head
z_D = dimensionless vertical distance, $zg/(v_G + v_L + w)^2$

Greek Letters

β = dimensionless area occupied by gas bubble, r_G^2/r_W^2
η = dimensionless radius, r/r_W
λ = cumulative volumetric liquid holdup
μ = liquid viscosity
ρ = liquid density
ϕ = functional dependence
Φ = functional dependence
Ψ = functional dependence
σ = surface tension

Subscripts

lim = liquid film when it has attained its limiting thickness

LITERATURE CITED

1. Davies, R. M., and G. I. Taylor, *Proc. Roy. Soc.*, **200A**, 375 (1950).
2. Dumitrescu, D. T., *Z. Angew. Math. Mech.*, **23**, 139 (1943).
3. Griffith, P., and G. B. Wallis, *Trans. Am. Soc. Mech. Engrs.*, **83C**, 307 (1961).
4. Laird, A. E. K., and D. Chisholm, *Ind. Eng. Chem.*, **48**, 1361 (1956).
5. Nicklin, D. J., Ph.D. thesis, Univ. of Cambridge, Cambridge, England (August, 1961).
6. Street, J. R., and M. R. Tek, *A.I.Ch.E.J.*, **11**, No. 4 (1965).
7. White, E. T., and R. H. Beardmore, *Chem. Eng. Sci.*, **17**, 351 (1962).
8. Bretherton, F. P., *J. Fluia Mech.*, **10**, 166 (1961).
9. Walters, J. K., and J. F. Davidson, *ibid.*, **12**, 408 (1962).
10. *Ibid.*, **17**, 321 (1963).
11. Taylor, T. D., and Andreas Acrivos, *ibid.*, **18.**, 466 (1964).
12. Brown, R. A. J., Ph.D. thesis, Univ. of Alberta, Edmonton, Alberta, Canada (May, 1963).
13. Hellums, J. D., and S. W. Churchill, *A.I.Ch.E. Journal*, **10**, 110 (1964).

Manuscript received May 15, 1964; revision received November 18, 1964; paper accepted January 22, 1965. Paper presented at A.I.Ch.E. Houston meeting.

Thermal Conductivity Measurements for Nitrogen in the Dense Gaseous State

DRAGOSLAV MISIC and GEORGE THODOS

Northwestern University, Evanston, Illinois

A coaxial cylindrical type of cell was designed and constructed for the measurement of the thermal conductivity of gases at high pressures and moderate temperatures. This cell was used to establish the thermal conductivity of nitrogen for pressures up to 4,625 lb./sq.in.abs. and for temperatures of 22.2° and 50.5°C. The resulting thermal conductivity values were found to be in agreement with values reported in the literature for nitrogen at these elevated pressures. These experimental measurements indicate that the cell developed for this investigation is capable of producing reliable thermal conductivities for gases at high pressures.

The transport properties of liquids and gases in the dense gaseous state are currently receiving considerable attention from both experimental and theoretical points of view. Predvoditelev (*36*) points out that the transfer of heat through a liquid medium possesses similar characteristics that are comparable to the transfer of heat through dense gases on the one hand and through solids on the other hand. Predvoditelev indicates that a generalized approach to the transport properties is possible. In 1881, Kamerlingh Onnes (*17*) introduced a normalizing parameter to produce a generalized viscosity correlation for gases at atmospheric pressure. Predvoditelev extends and refines this concept and applies it to the thermal conductivity of liquids. Chapman (*5*) and Enskog (*7*) independently developed, from rigorous kinetic theory considerations, expressions for the transport properties of the rare gases. For the effect of pressure on thermal conductivity, Enskog (*8*) presents the relationship

$$\frac{k}{k^*} = b\rho \left[\frac{1}{b\rho\chi} + \frac{6}{5} + 0.7574\, b\rho\chi \right] \qquad (1)$$